BNL-107272-2014-JA

NANO LETTERS

Subscriber access provided by BEIJING INST OF TECH

Communication

Sphere Shaped Hierarchical Cathode with Enhanced Growth of Nano-Crystal Planes for High-Rate and Cycling-Stable Li-Ion Batteries

Linjing Zhang, Ning Li, Borong Wu, Hongliang Xu, Lei Wang, Xiao-Qing Yang, and Feng Wu

Nano Lett., **Just Accepted Manuscript** • Publication Date (Web): 16 Dec 2014

Downloaded from http://pubs.acs.org on December 16, 2014

Just Accepted

"Just Accepted" manuscripts have been peer-reviewed and accepted for publication. They are posted online prior to technical editing, formatting for publication and author proofing. The American Chemical Society provides "Just Accepted" as a free service to the research community to expedite the dissemination of scientific material as soon as possible after acceptance. "Just Accepted" manuscripts appear in full in PDF format accompanied by an HTML abstract. "Just Accepted" manuscripts have been fully peer reviewed, but should not be considered the official version of record. They are accessible to all readers and citable by the Digital Object Identifier (DOI®). "Just Accepted" is an optional service offered to authors. Therefore, the "Just Accepted" Web site may not include all articles that will be published in the journal. After a manuscript is technically edited and formatted, it will be removed from the "Just Accepted" Web site and published as an ASAP article. Note that technical editing may introduce minor changes to the manuscript text and/or graphics which could affect content, and all legal disclaimers and ethical guidelines that apply to the journal pertain. ACS cannot be held responsible for errors or consequences arising from the use of information contained in these "Just Accepted" manuscripts.

ACS Publications
High quality. High impact.

Nano Letters is published by the American Chemical Society. 1155 Sixteenth Street N.W., Washington, DC 20036
Published by American Chemical Society. Copyright © American Chemical Society. However, no copyright claim is made to original U.S. Government works, or works produced by employees of any Commonwealth realm Crown government in the course of their duties.

Sphere Shaped Hierarchical Cathode with Enhanced Growth of Nano-Crystal Planes for High-Rate and Cycling-Stable Li-Ion Batteries

Linjing Zhang,[†,§] *Ning Li,*[†,§] *Borong Wu,**[,†,‡], *Hongliang Xu,*[†] *Lei Wang,*[†] *Xiao-Qing Yang,*[⊥] *and Feng Wu**[,†,‡]

[†]School of Chemical Engineering and the Environment, Beijing Institute of Technology, Beijing Key Laboratory of Environmental Science and Engineering Beijing, 100081, P. R. China.

[‡]Beijing Higher Institution Engineering Research Center of Power Battery and Chemical Energy Materials, Beijing, 100081, P. R. China.

[⊥]Chemistry Department, Brookhaven National Laboratory, Upton, NY, 11973, USA

ABSTRACT: High-energy and high-power Li-ion batteries have been intensively pursued as power sources in electronic vehicles and renewable energy storage systems in smart grids. With this purpose, developing high-performance cathode materials is urgently needed. Here we report an easy and versatile strategy to fabricate high-rate and cycling-stable hierarchical sphered cathode $Li_{1.2}Ni_{0.13}Mn_{0.54}Co_{0.13}O_2$, by using an ionic interfusion method. The sphere shaped hierarchical cathode is assembled with primary nano-plates with enhanced growth of nano-crystal planes in favor of Li^+ intercalation/deintercalation, such as (010), (100) and (110) planes. This material with such unique structural features exhibits outstanding rate capability,

cycleability and high discharge capacities, achieving around 70% （175 mAh g^{-1}） of the capacity at 0.1 C rate within about 2.1 minutes of ultrafast charging. Such cathode is feasible to construct high-energy and high-power Li-ion batteries.

KEYWORDS: Hierarchical spheres; Electrochemical active planes; Lithium-rich cathode; Li-ion batteries; High-rate; Cycling-stable.

Li-ion batteries (LIBs) are being intensively studied as high-energy and high-power sources for electric vehicles (EVs) and renewable energy storage in smart grids.[1-4] In order to expand these applications, the development of high-performance cathode materials is urgently needed.[5] Recently, layered lithium-rich (LLR) cathode materials, $x\mathrm{Li_2MnO_3}\cdot(1 - x)\mathrm{LiMO_2}$ ($0 < x < 1$, M = Ni, Mn, Co), have attracted great attentions since their first report,[6-10] due to their high capacities (*ca.* 250 mAh g^{-1}), low cost and environmental benignity.[11-13] They can be charged to a higher voltage (> 4.5 V) than the conventional cathode materials.[14-16] However, these layered oxides suffer from intrinsic poor rate capability, severe capacity fade and voltage decay, due to the rearrangement of surface structure caused by the activation of Li_2MnO_3 component above 4.5 V, the erosion from the electrolytes and the structural transformation during cycling.[17-19]

Many works have demonstrated that reducing particle sizes to nanoscale level can efficiently shorten the lithium-ions diffusion length,[20,21] but this may be detrimental to structural stability and promote severely undesired side reactions between electrode/electrolyte.[22] Based on this, hierarchical electrode materials, micro-assemblies composed of primary nanoparticles, have been developed to address these problems.[23-29] In our previous reported works, hierarchical nano/micro cathode materials have been proved to exhibit good electrochemical performance in

terms of discharge capacity and cycleability, yet the rate capability is pending enhancement.[25,26] Hence, individual hierarchical structure is not enough to yield high-energy and high-power cathodes.

Up to now, it has been widely reported that in hexagonal LLR oxides, Li^+ preferably moves two-dimensionally along the *a*-*b* planes ((001) planes), perpendicular to the *c*-axis. Therefore, if most parts of the nano-plate surface are parallel to (010), (100) and (110) planes, perpendicular to (001) plane, the rate of Li^+ intercalation/deintercalation will be significantly enhanced. This can be explained schematically by Scheme 1 as follows. Considering a crystal block formed by $10 \times 10 \times 10$ unit cells has two (001) surface planes on top and bottom and four side planes of (100) and (010) (Scheme 1A1). If a (001) nano-plate is obtained by cutting out a $10a \times 10b \times 2c$ piece parallel to (001) plane (Scheme 1A2), the total Li^+ entrance length will be $40a$, and the shotest diffusion length for Li^+ from edge to center will be $5a$. In cotrast, if the cutting is parallel to (010) plane (Scheme 1A3), the (010) nano-plate ($10a \times 2b \times 10c$ piece) will have total Li^+ entrance length of $24a \times 9 = 216a$, wich is more than 5 times longer than the (001) nano-plate. In addition, the shortest Li^+ diffusion length of $1a$ for (010) nano-plate is only 1/5 of $5a$ for (001) nano-plate. The (110) nano-plate yields similar advantage as the (100) and (010) plates. Therefore, the (100), (010) and (110) planes are called electrochemically active surface planes for Li^+ intercalation/deintercalation. Based on this, enhanced growth of these surface planes should be conducive to improve the rate capability.[30] Consequently, combination of the hierarchical structure and the enhanced growth of electrochemically active surface planes in favor of Li^+ intercalation/deintercalation, is feasible to hunt for integral performance of LLR cathodes. Unfortunately, the (010) (or (100)) planes with high surface energy trend to vanish

during crystal growth. To date, the synthesis of LLR materials with enhanced growth of such electrochemically active surface planes, remains a significant challenge.

In this communication, we report an easy and versatile strategy to fabricate $Li_{1.2}Ni_{0.13}Mn_{0.54}Co_{0.13}O_2$ (HS-LNMCO) cathode materials with hierarchical spheres as secondary particles, by using an ionic interfusion method. The secondary particles are assembled with primary nano-plate particles with enhanced growth of electrochemically active planes ((010), (100) and (110)). As illustrated in Scheme 1B, the urchin-like α-MnO_2 precursor can be obtained through the oxidation of Mn^{2+} by $S_2O_8^{2-}$ at room temperature, using $AgNO_3$ as catalyst. Then the precursor can be converted to the objective hierarchical structured spheres after interfused with Co^{2+}, Ni^{2+} and Li^+ salts and followed sintering process, via gas release and fracturing effect. The as-synthesized material has combined advantages of both (I) hierarchical architectures for secondary particles and (II) enhanced growth of electrochemically active surface planes for primary particles. In the primary particles, the nano-plates contain many exposed Li^+ electrochemically active surface planes, in favor of rapid Li^+ intercalation/deintercalation, and the micron-sized spherical shaped secondary particles with mesoporous can guarantee the structural stability and facilitate electrolyte penetration in the batteries. It is demonstrated that, when tested as cathode for LIBs, this HS-LNMCO electrode manifests outstanding rate capability, excellent cycle stability and high discharge capacity.

Scheme 1. The shcematic diagram of the HS-LNMCO cathode.

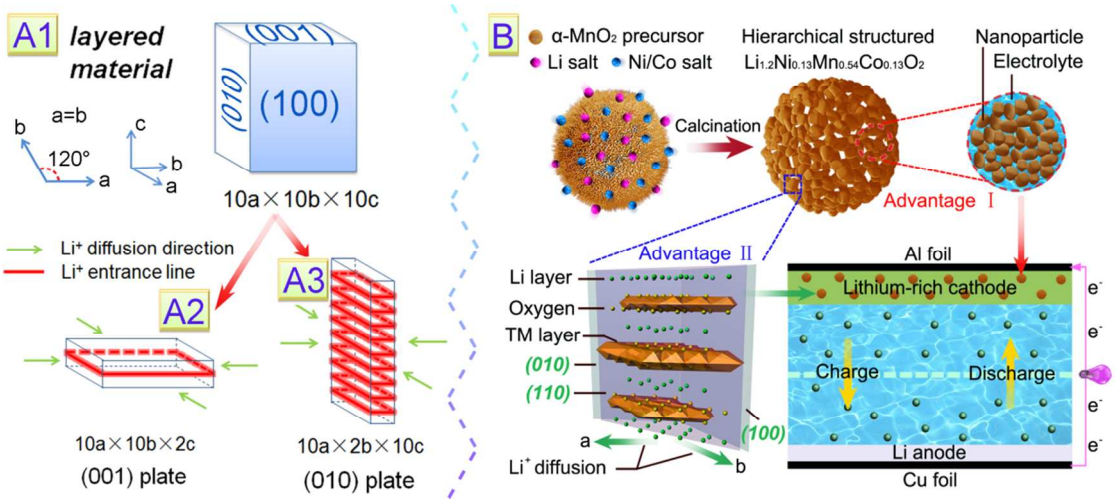

To optimize synthesis conditions of the urchin-like α-MnO_2 precursors, time-dependent evolution processes (12, 24, 36, and 48 h) are applied. Filed-emission scanning electron microscopy (FESEM) images (Figure S1 in Supporting Information) indicate that the sample reacted for 24 h, labeled as M24, yields the most uniform and mono-dispersed spheres. Its corresponding powder X-ray diffraction (XRD) patterns, transmission electron microscopy (TEM) and high-resolution TEM (HRTEM) images are shown in Figure 1. The crystal structure of the M24 precursor can be indexed to a pure tetragonal phase (JCPDS 44-0141, Figure 1a).[31] As revealed in Figure 1b, these urchin-like α-MnO_2 spheres possess diameters of about 2 - 4 μm, and abundant nanorods are densely aligned on their surface (inset). The detailed microstructure of the nanorods is clearly displayed in Figure 1c. They are mainly isolated except for some intergrown ones, with 5 - 20 nm in diameter and several hundred nanometers in length. This structure can provide not only enough surface areas for homogenous distribution of transition metal (TM) salts on the α-MnO_2 precursor, but also particles agglomeration prevention.

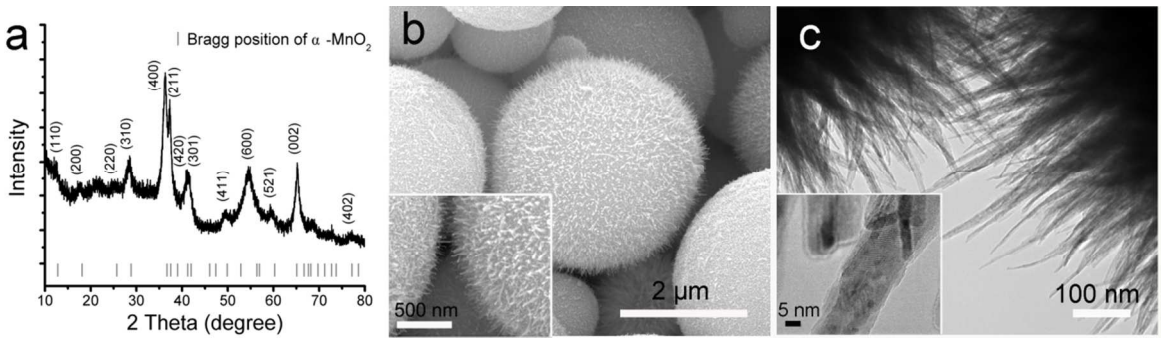

Figure 1. (a) XRD patterns; (b) FESEM images and (inset) magnified FESEM images of the α-MnO_2 precursor; (c) typical TEM images and (inset) HRTEM images of the nanorods on the α-MnO_2 precursor.

After chemical lithiation and calcination, the HS-LNMCO, $Li_{1.2}Ni_{0.13}Mn_{0.54}Co_{0.13}O_2$, was obtained. The morphology of the HS-LNMCO sample is examined in Figure 2. In Figure 2a, it is apparent that micron-sized and spherical shaped features are preserved after annealing process, which is quite suitable for battery fabrication. Meanwhile, there is a little increase in particle sizes compared with the α-MnO_2 precursor, with an average diameter of 3 - 5 μm. It may be caused by gas release and fracturing effect. However, noticeable variations are visible, for example, each spherical secondary particle is constructed of small primary nano-plates with average width of 200 - 400 nm. In addition, inner mesopores are clearly evident within the micro-sized secondary particles, as shown in Figure 2b. The more exact microstructure is investigated by TEM images. The hierarchically spherical and mesoporous structure is further confirmed by Figure 2c, 2d. The mesopores can provide not only more active surface areas for high-efficiency electrochemical reaction, but also electrolyte penetration into the material particles, as shown in Scheme 1. Pore size distribution in Figure S2 shows that the average pore size is approximately 10 nm. The primary nano-plate characteristics in hierarchical structure are verified by red and green dotted circles in Figure 2e, 2f and Figure S3. Energy dispersive X-ray

spectroscopy (EDX) and X-ray photoelectron spectroscopy (XPS) results (Figure S4) of the HS-LNMCO suggest the uniform distributions of Ni, Mn, Co and O elements and the oxidation states of Ni, Mn and Co are +2, +4 and +3.[32]

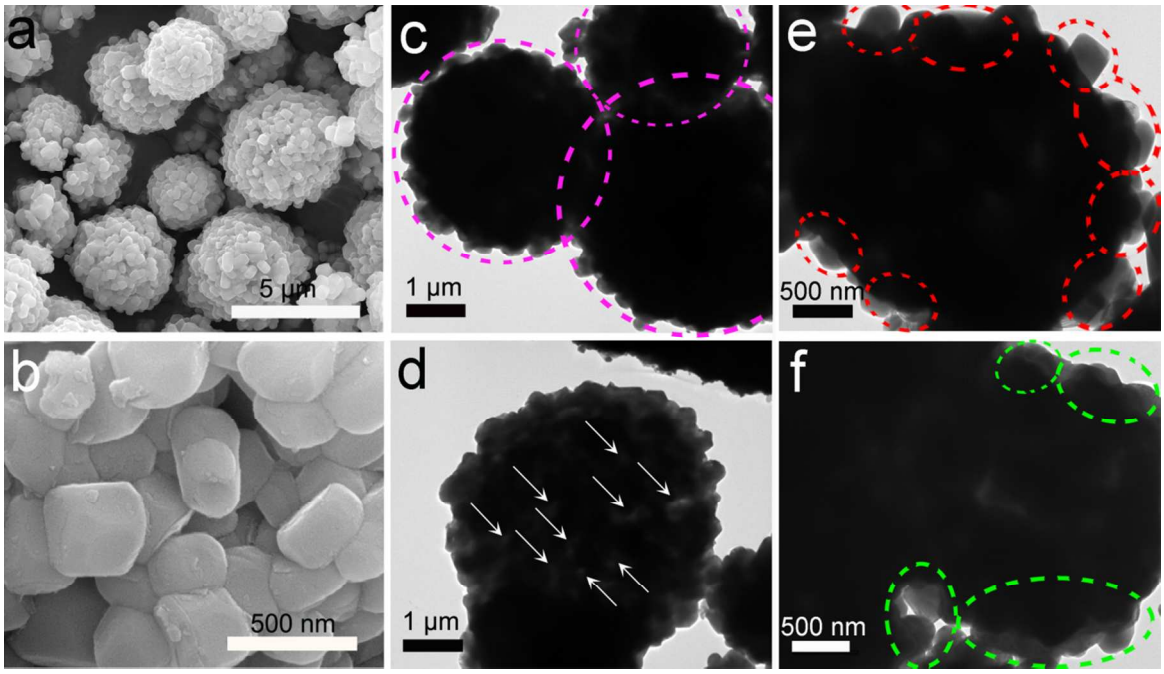

Figure 2. (a) FESEM image; (b) magnified FESEM image; (c-f) typical TEM image of the HS-LNMCO.

To serve as reference for comparison, the $Li_{1.2}Ni_{0.13}Mn_{0.54}Co_{0.13}O_2$ material was also synthesized using a sol-gel method in this paper, labeled as SG-LNMCO. The structural characterization XRD patterns of both materials are plotted in Figure 3. Pure phase is observed in the XRD patterns. All the peaks of both samples can be indexed with a hexagonal α-$NaFeO_2$ structure (space group, *R*-3*m*), except for the weak reflection peaks between 20° and 25°, which are characteristics of the superlattice structure (space group, *C*/2*m*).[6,11,14,15] The splitting of (006)/(012) and (018)/(110) indicates their well-crystallized layered structure. It is interesting to note that the intensity of (110) peak is obviously stronger than the (018) peak for the HS-

LNMCO sample. In contrast, for the SG-LNMCO, the intensities of the two peaks are almost the same, similar to that reported in previous literatures.[11-13,24-26] According to the calculated results from the XRD patterns, the ratio values of $I_{(110)}/I_{(018)}$ for the HS-LNMCO (K_{HS} = 1.25) is 1.24 times of that for the SG-LNMCO (K_{SG} = 1.04). The results clearly imply the enhanced growth of the (110) planes in the HS-LNMCO compared with that in the SG-LNMCO. Since the (100) and (010) peaks can not be observed for the α-$NaFeO_2$ structure (space group, *R*-3*m*) due to the crystal extinction, the only experimental evidence obtained from XRD patterns is the intensity ratio of $I_{(110)}/I_{(018)}$, which is not sufficient. Therefore, the HRTEM analysis was performed to provide further more experimental evidence as described later.

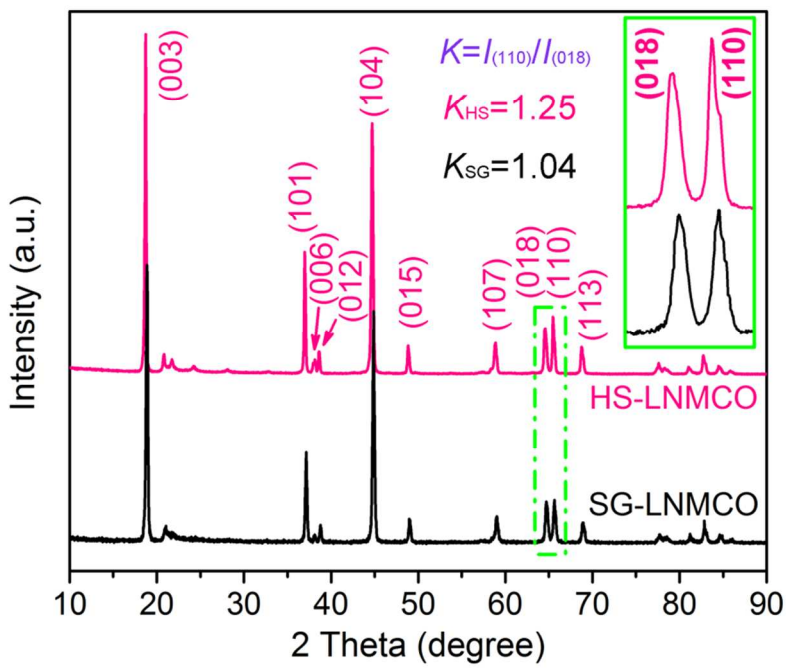

Figure 3. XRD patterns of the HS-LNMCO and the SG-LNMCO.

To elucidate the accurate characteristics of the primary nano-plates, HRTEM characterization and the selected area electron diffraction (SAED) studies of the HS-LNMCO material were carried out and the results are shown in Figure 4. Mesoporous are further confirmed in Figure 4a.

Several primary nano-plates are obviously shown in Figure 4b using high magnification. HRTEM images from two different plates (region i and region ii) are displayed in Figure 4c - 4f. In both two regions, the apparent lattice fringes with interplanar spacing of 0.47 nm, are clearly observed. These fringes are assigned to the planar distance between (003) planes of LLR material, implying that the projected image planes of the primary nano-plates are parallel to the *c*-axial direction (parallel to (100), (010), or (110) planes). Such characteristics fringes can be frequently observed in the investigation of primary nano-plates of the HS-LNMCO material, but relatively difficult to be observed in the SG-LNMCO material. The SAED patterns in Figure 4g, confirm that the frontal plane observed in region (i) is the (010) plane. As mentioned previously, Li^+ diffuses along two-dimensional pathway perpendicular to (010) plane in the layered structure (inset of Figure 4g). For comparison, the HRTEM image of the SG-LNMCO particles was also examined, as shown in Figure 4h. The fast Fourier transform algorithm (FFT) result (inset of Figure 4h) of the region in white square indicates the six-fold symmetry characteristics of the SG-LNMCO. And the frontal plane observed is the (001) plane, which is not beneficial for Li^+ diffusion. Therefore, we can conclude with confidence that the enhanced growth of electrochemically active surface planes in favor of Li^+ intercalation/deintercalation has been successfully achieved for the HS-LNMCO material. The as-obtained HS-LNMCO material with enhanced growth of (100) and (010) surface planes, has superior inherent Li^+ intercalation/deintercalation kinetics, great rate capability and high power density.

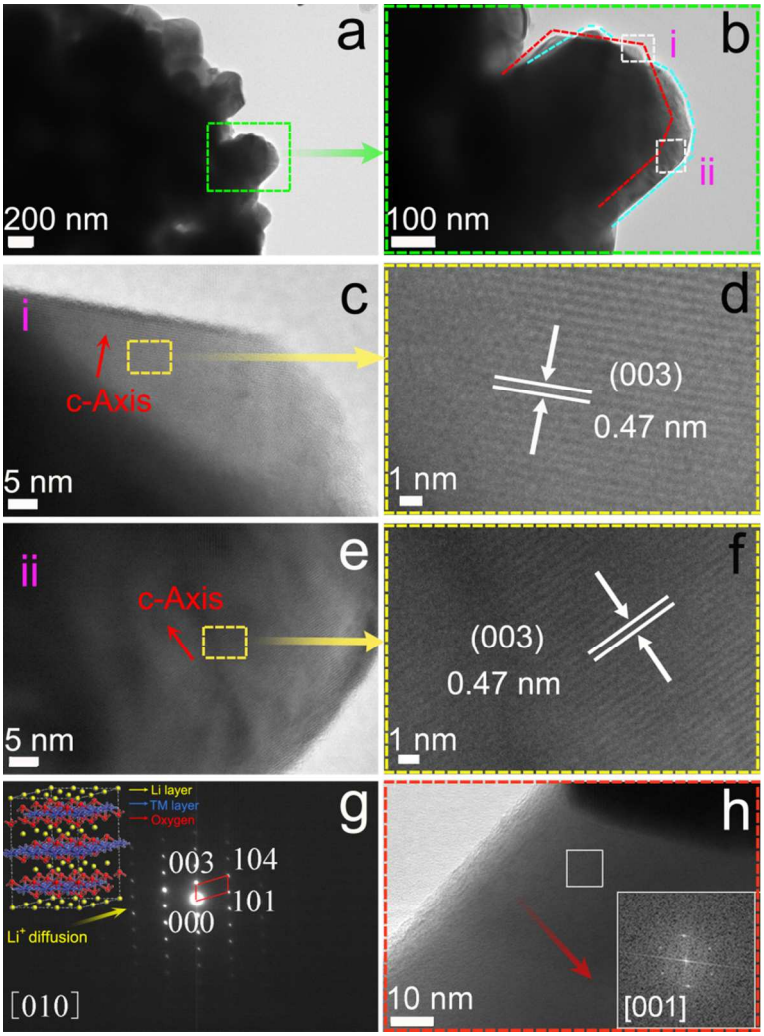

Figure 4. (a,b) Typical TEM images; (c-f) HRTEM images of the nano-plates in the HS-LNMCO; (g) the corresponding SAED patterns of the region (i), and (inset) schematic diagrams of Li^+ diffusion in LLR cathodes; (h) HRTEM of the SG-LNMCO and (inset) Fast Fourier Transform Algorithm (FFT) result of the region in white square.

The advantages of the HS-LNMCO material in terms of electrochemical performance were studied, cycled at a constant current density 25 mA g^{-1} (0.1 C) as shown in Figure 5a, and the mass loading of HS-LNMCO material is about 2.8 - 3.0 mg cm^{-2} in the electrode. The HS-LNMCO material derived from M24 (Figure S5), displays the highest initial discharge capacity among all the lithium-rich materials derived from α-MnO_2 precursors reacted for different time

(12 h, 24 h, 36 h and 48 h). The inset of Figure 5a presents the corresponding charge/discharge profiles of the HS-LNMCO material. There is a long plateau around 4.5 V on the initial charging, due to the irreversible Li_2O exaction from the Li_2MnO_3 component.[33] The voltage decay can be seen during cycling due to phase transformation.[15,21,34,35] It is worth noticing that the HS-LNMCO material shows a discharge capacity of around 250 mAh g^{-1} after 50 cycles, with excellent capacity retention of 97 % and coulombic efficiency of almost 100 %, indicating its extremely good electrochemical reversibility. This is also verified by the cyclic voltammograms (CVs) results in Figure S6. Such excellent cycling performance is probably attributed to the structural stability of micron-sized, hierarchical sphere-shaped secondary particles. Moreover, the mesoporous structure of this material may also contribute to the high reversibility by providing good contact between electrolyte and inner particles.

To further demonstrate the advantages of the hierarchical structure and enhanced growth of electrochemically active surface planes, long-term cycling performance of the HS-LNMCO material at different high C - rates were studied and the results are shown in Figure 5b. The cells were charged at 250 mA g^{-1} (1 C) first, followed by a constant voltage charge at 4.8 V, and then discharged at 250 mA g^{-1} (1 C), 500 mA g^{-1} (2 C) and 1250 mA g^{-1} (5 C), after initially activation cycled for 3 cycles at 0.1 C, respectively. Note that discharge capacities gradually increase during cycling, due to further activation of the hierarchical structured cathode material at 1 C rate, which is testified by the charge transfer resistance (Rct) variation (Figure S7, Table S1). Figure 5b and Figure S8 show that, at 1 C rate charging, the HS-LNMCO cathode yields maximal discharge capacities of 228.6, 202.9 and 180.6 mAh g^{-1} at 1 C, 2 C and 5 C, respectively; and even retains over 90 % at all rates at the completion of 100 cycles, with coulombic efficiencies of approximately 100 %. Figure S9 shows the corresponding charge and

discharge profiles of the HS-LNMCO electrodes. However, the SG-LNMCO tested for comparison shows poor rate capability and severe capacity fade, and retains only about 40% of capacity at 0.1 C rate, as shown in Figure S10. These results demonstrate the outstanding rate capability and cycleability of the HS-LNMCO cathode at high-rates. The FESEM images (Figure 5b and Figure S11) of the cycled electrodes reveal that the hierarchical structured microspheres are well preserved over long-term cycling, indicating their good structural stability.

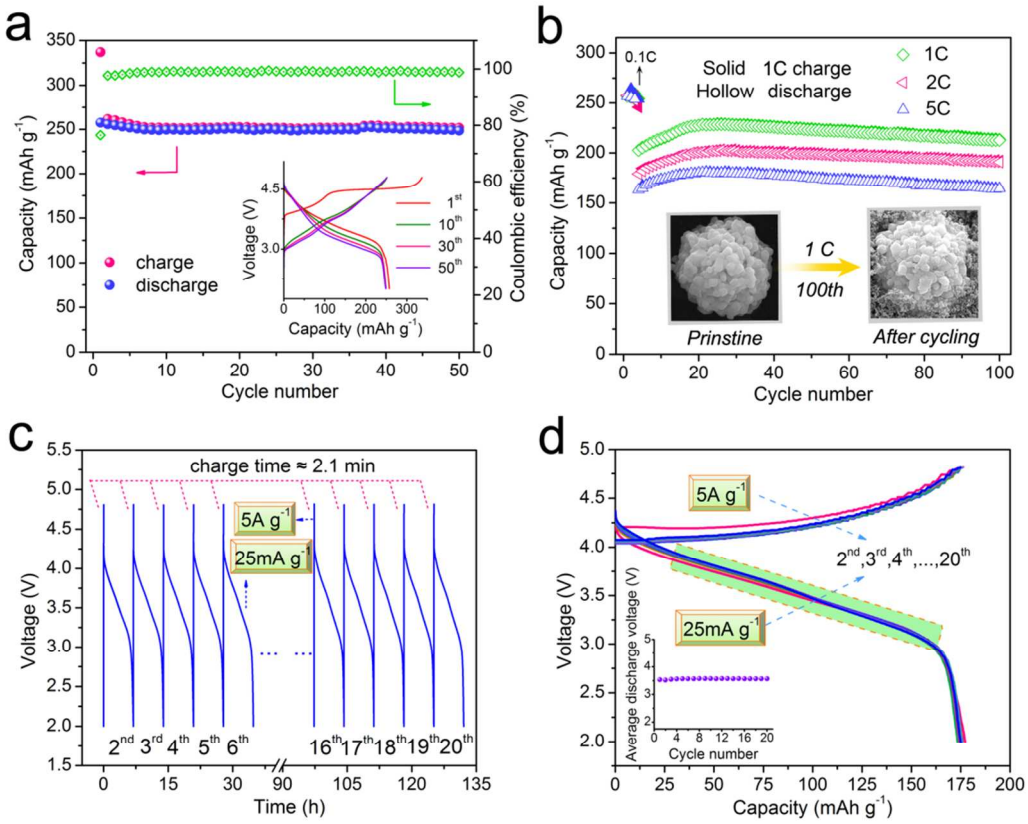

Figure 5. Electrochemical performance of the coin type cells with the HS-LNMCO cathodes cycled in the range of 2.0 - 4.8 V *vs.* Li^+/Li. (a) Cycling performance at constant current density of 0.1 C (1 C = 250 mA g^{-1}), and (inset) charge/discharge profiles; (b) cycling performance, charged at 1 C and discharged at 1 C, 2 C and 5 C, and FESEM images of prinstine material and cycled electrode for 100 cycles at 1 C, respectively; (c,d) ultra-fast charge capability, charged at 20 C and then discharged at 0.1 C, and (inset of d) average discharge voltage *vs.* cycle number.

Take practical application into consideration, where short charge time is in demand, the cells were tested at ultrahigh current density of 5 A g^{-1} (20 C) for charge and lower current density of 25 mA g^{-1} for discharge after activated for 1 cycle (Figure 5c, 5d). Surprisingly, with only about 2.1 minutes of charge time, the HS-LNMCO material achieves a capacity of 177.3 mAh g^{-1} initially, and a capacity as high as 175.0 mAh g^{-1} (70% of the capacity at 0.1C rate) can be maintained even after 20 cycles, which is among the highest value of such materials.[6,11,24,30,34] Remarkably, negligible voltage drop can be observed in discharge profiles as well, suggesting the good structural stability of the HS-LNMCO material at high-rates. High discharge capacities, shortened charge time and less voltage fade are also observed at 1.25 A g^{-1} (5 C) and 2.5 A g^{-1} (10 C) for charge (Figure S12). This outstanding performance in terms of shortened charge time, voltage stability and high capacities are just what we are looking for in developing the power sources for EVs applications. It is believed that such excellent performance is mainly originated from the novel hierarchical structured spheres and enhanced growth of electrochemically active surface planes of the HS-LNMCO, that is (100), (010) and (110) planes. The primary nanoparticles with enhanced growth of electrochemically active surface planes, promise ultrafast Li^+ intercalation/deintercalation as well as Li^+ diffusion, while the micro-assemblies with mesopores, ensure the good structural stability and good penetration of the electrolyte into the electrodes even at high current densities. This uniquely architectured cathode may be stable enough to respond and tolerate to ultrahigh rate charing process and maintains layered structue well after ultrafast Li^+ extraction and diffusion. Consequently, at fast charging, the voltage fade, generally caused by layered-to-spinel structural transformation during cycling[10,12,13,34-36], can be possibly alleviated for the layered lithium-rich cathode with ultrafast Li^+ intercalating/deintercalating and Li^+ diffusing kinetics.

In conclusion, we have developed a new approach to synthesize novel sphere shaped hierarchical cathode $Li_{1.2}Ni_{0.13}Mn_{0.54}Co_{0.13}O_2$ with enhanced growth of crystal planes in favor of Li^+ intercalation/deintercalation. This unique architecture endows the material with ultrafast Li^+ intercalation/deintercalation as well as diffusion kinetics and excellent structural stability, yielding outstanding electrochemical properties in terms of rate capability, cycleability and capacity. The results clearly demonstrate the promising application of sphere shaped hierarchical cathode in high-rate and cycling-stable LIBs, which are very important for the development of power sources for EVs applications. Meanwhile, the simple synthesis strategy used in this work is expected to inspire further development of other functional electrochemical materials.

ASSOCIATED CONTENT

Detail of experimental and additional figures depicting experiment results. This material is available free of charge via the Internet at http://pubs.acs.org.

AUTHOR INFORMATION

Corresponding Author

*(B.W.) E-mail: borongwu@gmail.com.

*(F.W.) E-mail: wufeng863@vip.sina.com.

Author Contributions

[§]L.Z. and N.L. contributed equally to this work. L.Z. conceived the idea, designed the experiments and discussed with B.W. and F.W.; L.Z. and N.L. carried out the experiments and analyzed the data; L.Z., N.L., B.W., X.-Q.Y. and F.W. wrote and revised the manuscript. All authors participated in discussions of the research.

Notes

The authors declare no competing financial interest.

ACKNOWLEDGMENT

The authors greatly appreciate the financial support from National 863 Program (2013AA050903) of China, Beijing Key Laboratory of Environmental Science and Engineering (20131039031), Beijing Higher Institution Engineering Research Center for Power Battery and Chemical Energy Materials (2012039032), National Natural Science Foundation of China (21443013). The work done at Brookhaven National Lab. is supported by the Assistant Secretary for Energy Efficiency and Renewable Energy, Office of Vehicle Technologies, under the program of Vehicle Technology Program, under Contract Number DEAC02-98CH10886.

REFERENCES

(1) Armand, M.; Tarascon, J. M. *Nature* **2008**, *451*, 652-657.

(2) Sun, Y.-K.; Myung, S.-T.; Park, B.-C.; Prakash, J.; Belharouak, I.; Amine, K. *Nat. Mater.* **2009**, *8*, 320-324.

(3) Whittingham, M. S. *Chem. Rev.* **2004**, *104*, 4271-4301.

(4) Goodenough, J. B.; Park, K. S. *J. Am. Chem. Soc.* **2013**, *135*, 1167-1176.

(5) Lee, E.-S.; Huq, A.; Chang, H.-Y.; Manthiram, A. *Chem. Mater.* **2012**, *24*, 600-612.

(6) Lu, Z.; MacNeil, D. D.; Dahn, J. R. *Electrochem. Solid-State Lett.* **2001**, *4*, A191-A194.

(7) Ammundsen, B.; Paulsen, J. *Adv. Mater.* **2001**, *13*, 943-956.

(8) Hong, Y.-S.; Park, Y. J.; Ryu, K. S.; Chang, S. H.; Kim, M. G. *J. Mater. Chem.* **2004**, *14*, 1424-1429.

(9) Lei, C.H.; Bareño, J.; Wen, J.G.; Petrov, I.; Kang, S.-H.; Abraham, D. P. *J. Power Sources* **2008**, *178*, 422-433.

(10) Johnson, C. S.; Li, N.; Lefief, C.; Vaughey, J. T.; Thackeray, M. M. *Chem. Mater.* **2008**, *20*, 6095-6106.

(11) Lu, Z.; Beaulieu, L. Y.; Donaberger, R. A.; Thomas, C. L.; Dahn, J. R. *J. Electrochem. Soc.* **2002**, *149*, A778-A791.

(12) Wu, F.; Li, N.; Su, Y.; Shou, H.; Bao, L.; Yang, W.; Zhang, L.; An, R.; Chen, S. *Adv. Mater.* **2013**, *25*, 3722-3726.

(13) Wu, F.; Li, N.; Su, Y.; Zhang, L.; Bao, L.; Wang, J.; Chen, L.; Zheng, Y.; Dai, L.; Peng, J.; Chen, S. *Nano Lett.* **2014**, *14*, 3550-3555.

(14) Armstrong, A. R.; Holzapfel, M.; Novak, P.; Johnson, C. S.; Kang, S.-H.; Thackeray, M. M.; Bruce, P. G. *J. Am. Chem. Soc.* **2006**, *128*, 8694-8698.

(15) Thackeray, M. M.; Kang, S.-H.; Johnson, C. S.; Vaughey, J. T.; Hackney, S. A. *Electrochem. Commun.* **2006**, *8*, 1531-1538.

(16) Yabuuchi, N.; Yoshii, K.; Myung, S.-T.; Nakai, I.; Komaba, S. *J. Am. Chem. Soc.* **2011**, *133*, 4404-4419.

(17) Xu, B.; Fell, C. R.; Chi, M.; Meng, Y. S. *Energy Environ. Sci.* **2011**, *4*, 2223-2233.

(18) Mohanty, D.; Kalnaus, S.; Meisner, R. A.; Rhodes, K. J.; Li, J.; Payzant, E. A.; Wood III, D. L.; Daniel, C. *J. Power Sources* **2013**, *229*, 239-248.

(19) Boulineau, A.; Simonin, L.; Colin, J.-F.; Bourbon, C.; Patoux, S. *Nano Lett.* **2013**, *13*, 3857-3863.

(20) Aricò, A. S.; Bruce, P.; Scrosati, B.; Tarascon, J.-M.; van Schalkwijk, W. *Nat. Mater.* **2005**, *4*, 366-377.

(21) Kim, M. G.; Jo, M.; Hong, Y.-S.; Cho, J. *Chem. Commun.* **2009**, 218-220.

(22) Guo, Y.-G.; Hu, J.-S.; Wan, L.-J. *Adv. Mater.* **2008**, *20*, 2878-2887.

(23) Zhou, L.; Zhao, D.; Lou, X. W. (David) *Angew. Chem. Int. Ed.* **2012**, *51*, 239-241.

(24) Wang, D.; Belharouak, I.; Zhou, G.; Amine, K. *Adv. Funct. Mater.* **2013**, *23*, 1070-1075.

(25) Zhang, L.; Wu, B.; Li, N.; Mu, D.; Zhang, C.; Wu, F. *J. Power Sources* **2013**, *240*, 644-652.

(26) Zhang, L.; Wu, B.; Li, N.; Wu, F. *Electrochim. Acta* **2014**, *118*, 67-74.

(27) Hercule, K. M.; Wei, Q.; Khan, A. M.; Zhao, Y.; Tian, X.; Mai, L. *Nano Lett.* **2013**, *13*, 5685-5691.

(28) Yi, R.; Dai, F.; Gordin, M. L.; Chen, S.; Wang, D. *Adv. Energy Mater.* **2013**, *3*, 295-300.

(29) Xiao, J.; Wan, L.; Yang, S.; Xiao, F.; Wang, S. *Nano Lett.* **2014**, *14*, 831-838.

(30) Wei, G.-Z.; Lu, X.; Ke, F.-S.; Huang, L.; Li, J.-T.; Wang, Z.-X.; Zhou, Z.-Y.; Sun, S.-G. *Adv. Mater.* **2010**, *22*, 4364-4367.

(31) Li, Z.; Ding, Y.; Xiong, Y.; Yang, Q.; Xie, Y. *Chem. Commun.* **2005**, 918-920.

(32) Abouimrane, A.; Compton, O. C.; Deng, H.; Belharouak, I.; Dikin, D. A.; Nguyen, S. T.; Amine, K. *Electrochem. Solid State Lett.* **2011**, *14*, A126-A129.

(33) Hy, S.; Felix, F.; Rick, J.; Su, W.-N.; Hwang, B. J. *J. Am. Chem. Soc.* **2014**, *136*, 999-1007.

(34) Sun, Y.-K.; Lee, M.-J.; Yoon, C. S.; Hassoun, J.; Amine, K.; Scrosati, B. *Adv. Mater.* **2012**, *24*, 1192-1196.

(35) Wu, F.; Li, N.; Su, Y.; Lu, H.; Zhang, L.; An, R.; Wang, Z.; Bao, L.; Chen, S. *J. Mater. Chem.* **2012**, *22*, 1489-1497.

(36) Gu, M.; Belharouak, I.; Zheng, J.; Wu, H.; Xiao, J.; Genc, A.; Amine, K.; Thevuthasan, S.; Baer, D. R.; Zhang, J.-G. *ACS Nano* **2013**, *7*, 760-767.
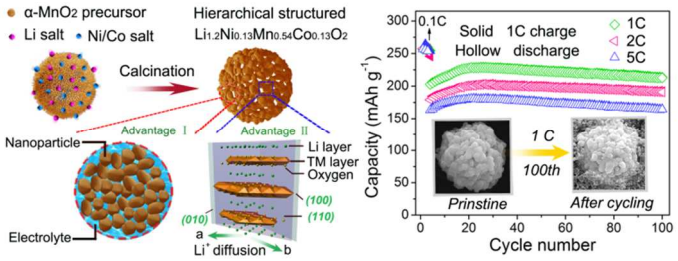
TABLE OF CONTENTS GRAPHIC.